

EPR of Gd^{3+} -metal-ion complexes in CaF_2 , BaF_2 , and SrCl_2

E. J. Bijvank and H. W. den Hartog

Solid State Physics Laboratory, 1 Melkweg, Groningen, The Netherlands

J. Andriessen

Department of Applied Physics, Technische Hogeschool Delft, Delft, The Netherlands

(Received 25 February 1977)

EPR experiments of Gd^{3+} - M^+ complexes in CaF_2 , BaF_2 , and SrCl_2 crystals are reported. We have studied the effect of the excess negative charge of the metal-ion impurity on the crystal field; also the relaxations of the halide ions neighboring the complex have been investigated. It will be shown that the values of the second-degree crystal-field parameters as determined from the EPR spectra can be explained in terms of an extended-point-charge model. For the calculations of the magnetic parameters we have taken into account second-order effects of odd crystal-field terms which have also been calculated using the point-ion-lattice model. Distortions of the lattice surrounding the Gd^{3+} - M^+ complexes are found to have large effects on the magnitude of the second-degree crystal-field parameters. Our experimental results have also been interpreted on the basis of the superposition model in which it is assumed that the crystal-field parameters are determined by the nature and positions of the nearest neighbors of the Gd^{3+} impurity. It will be shown in this paper that for Gd^{3+} - M^+ complexes in CaF_2 the superposition model predicts unrealistically large displacements of the fluorine ions neighboring the Gd^{3+} and M^+ impurity.

I. INTRODUCTION

Trivalent gadolinium ions, which have substituted for divalent cations in alkaline-earth halides, can be considered as excess positive charges with respect to the crystal lattice. In otherwise pure crystals these effective charges give rise to compensation by charges of opposite sign. Charge compensation of this type has been studied by various techniques such as dielectric relaxation,¹⁻³ EPR,^{4,5} and optical spectroscopy.⁶ In the present paper we shall be interested in a different form of charge compensation. Here, the compensating entities are monovalent impurity ions which represent excess negative charges when substituted for divalent cations.

Depending upon the association energy of the compensating defects the charge compensation can be either local or nonlocal. Local charge compensation is characterized by the existence of dipolar complexes. An example of the complexes studied in this paper has been shown in Fig. 1.

The structure of the crystalline hosts employed in this investigation is of the fluorite type. It consists of two sublattices: the halide sublattice is simple cubic; the cations are located in the centers of alternate cubes of halide ions. When the trivalent and monovalent impurities are nearest neighbors (local charge compensation) as shown in Fig. 1 we have an orthorhombic complex; the point symmetry at the Gd^{3+} site is C_{2v} . The principal axes x , y , and z have been chosen along the crystallographic directions $[001]$, $[110]$, and $[\bar{1}10]$, respectively. For this particular choice of the

principal axes we can write for the spin Hamiltonian associated with the $4f^7$ electron system of Gd^{3+} (see also Mims⁷):

$$\mathcal{H} = g\mu_B \vec{H} \cdot \vec{S} + B_2^0 O_2^0 + B_2^2 O_2^2 + B_4^0 O_4^0 + B_4^2 O_4^2 + B_4^4 O_4^4 + B_6^0 O_6^0 + B_6^2 O_6^2 + B_6^4 O_6^4 + B_6^6 O_6^6, \quad (1)$$

where the first term on the right-hand side accounts for the Zeeman interaction. The remaining terms are associated with crystal field interactions due to the surrounding lattice. The crystal-field operators O_l^m have been given by Abragam and Bleaney.⁸ When the principal axes x , y , and z are chosen as shown in Fig. 1, instead of along the $\langle 100 \rangle$ axes, the spin Hamiltonian of cubic Gd^{3+} consists of the Zeeman term and the fourth and sixth-degree crystal-field terms as given in (1). The excess negative charge of the monovalent

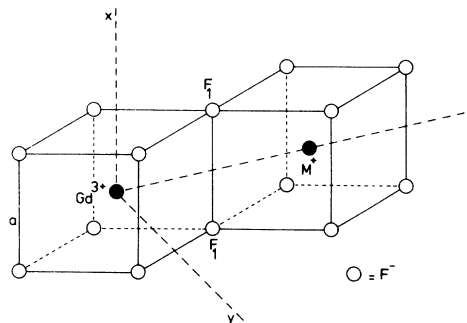


FIG. 1. Three-dimensional schematic representation of a Gd^{3+} - M^+ complex in CaF_2 . The principal axes x , y , and z have been indicated.

cation neighboring the Gd^{3+} ion will produce an extra term to the crystal field at the Gd^{3+} as compared to the cubic crystal field. This additional contribution will be of the form $B_2^0 O_2^0$; the excess charge does not contribute to the term $B_2^0 O_2^0$. Distortions of the lattice surrounding the Gd^{3+} impurity and polarization of nearby ions in general give rise to both second degree terms in (1).

When we choose for the extra impurity of the Gd^{3+} - M^+ complex the various alkali ions Li^+ , Na^+ , K^+ , Rb^+ , and Cs^+ the effective negative charge is -1 for all cases, however the distortion due to the misfit of the ionic radii of the impurity ions and the host crystal cations will increase on going from Li^+ to Cs^+ . In agreement with the line of reasoning given above we have observed drastic changes of the spin-Hamiltonian parameters B_2^0 and B_2^2 for the various complexes of the type Gd^{3+} - M^+ in CaF_2 . For Gd^{3+} - Li^+ and Gd^{3+} - Cs^+ we have found for B_2^0 , 14.9 and 220.5 G, respectively, and for B_2^2 , -49.1 and -4.0 G, respectively. These variations indicate that the experimental method employed here is capable of determining extremely small lattice distortions.

The experimental values of B_2^m in Eq. (1) obtained from the EPR spectra can be connected with the electrostatic crystal-field potential. The mechanisms giving rise to the zero-field splittings of the $^8S_{7/2}$ level of Gd^{3+} in crystalline hosts have been discussed by many authors in the literature.⁹⁻¹² We shall employ here the mechanisms proposed by Hutchison *et al.*⁹ and Wybourne¹⁰ for the calculation of B_2^0 and B_2^2 . When these coupling mechanisms are connected with an extended point-ion lattice approximation, in which the surrounding lattice consists of polarizable point charges, one obtains fair agreement between theory and experiment for B_2^0 and B_2^2 of the systems $BaCl_2:Gd^{3+}$, $BaCl_2:Eu^{2+}$, $PbCl_2:Gd^{3+}$, and $PbCl_2:Eu^{2+}$ (Refs. 13-16). In an earlier paper on orthorhombic Gd^{3+} - M^+ complexes in $SrCl_2$ we have shown, that with the point charge model one is able to explain the values of B_2^0 and B_2^2 .

It should be emphasized however that the explanation of the second degree spin-Hamiltonian parameters is not always as straightforward as suggested above. This has led Newman and co-workers^{12,17} to propose empirical power laws for the calculation of the B_2^m 's. These power laws are particularly successful in explaining the spin-Hamiltonian parameters for Gd^{3+} in host crystals containing oxygen ligands such as the zircon-structure compounds and scheelite hosts.¹⁷ In the case of fluorites this model has been used to explain experimental spin-Hamiltonian parameters on the basis of local distortion effects; for Gd^{3+} at rhombic sites in CaF_2 the intrinsic parameters occurring

in the model have been determined.¹⁸ We shall show in Sec. V that the model introduced by Newman (the superposition model) yields extremely large distortions, leading to an inconsistency because the power laws only hold for small distortions.

A comparison between the results obtained using the electrostatic model and the superposition model shows that the distortions necessary to explain the second-degree spin-Hamiltonian parameters are much smaller on the basis of the former treatment. In fact the distortions calculated using the point-charge model are quite well understandable in view of the differences between the ionic radii of the monovalent cation impurities and the divalent ions of the host crystal.

II. EXPERIMENTAL PROCEDURES

For the preparation technique used for the production of the $SrCl_2$ crystals we refer to an earlier paper.¹⁹ In $SrCl_2$ crystals doped with equal concentrations of Gd^{3+} and Na^+ ions about 50% of the Gd^{3+} impurities was compensated by Na^+ ions.

The CaF_2 and BaF_2 crystals were grown by a modified Bridgman technique in a high-frequency furnace under a purified He atmosphere. Spectroscopically pure carbon was used as crucible material. In order to be certain that sufficient concentrations of compensated Gd^{3+} ions were present the growth rate was limited to 6 mm/h. The Gd^{3+} and M^+ ions were added as fluorides.

Prior to crystal growth we prepared a boule of polycrystalline CaF_2 and BaF_2 from powder. The powder was heated very slowly in high vacuum (10^{-6} Torr) in order to remove the adsorbed H_2O and O_2 molecules; (1-2)% PbF_2 was added to act as scavenger; it is known that PbF_2 reduces the concentrations of O^{2-} and OH^- impurities considerably.

The spin-Hamiltonian parameters B_2^m have been determined from the rotational diagrams by means of a least-squares-fitting procedure. Because in some cases we are dealing with crystal-field splittings which are not small as compared to the Zeeman energy we have diagonalized the spin Hamiltonian for each angle between the magnetic field direction and the principal axes at the specific magnetic field strength. The method used here is similar to the one proposed by Uhrin.²⁰

The EPR experiments were carried out with a Varian E3 X-band EPR spectrometer. Most of the experiments were performed at room temperature. The temperature-dependent experiments were carried out with a LN_2 (liquid-nitrogen)-flow cryostat.

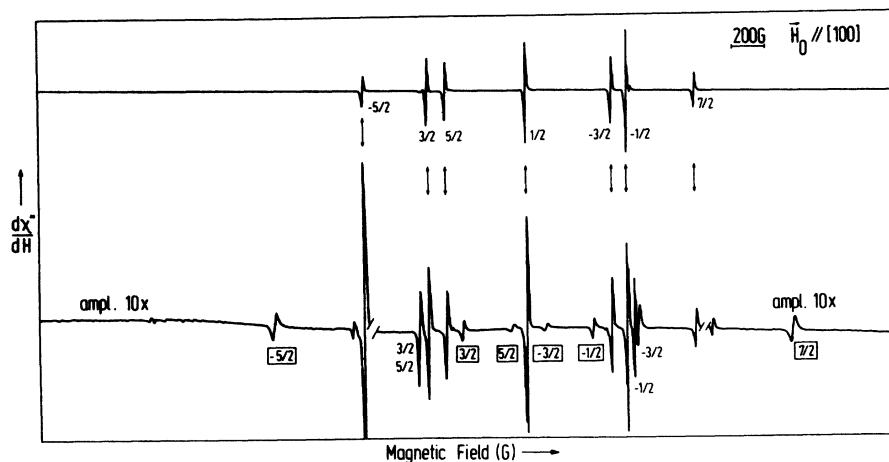


FIG. 2. EPR spectra of $\text{CaF}_2:\text{Gd}^{3+}$ (upper signal) and $\text{CaF}_2:\text{Gd}^{3+}, \text{Li}^+$ (lower signal) for $\vec{H}_0 \parallel [100]$ measured at 300 K. The EPR lines associated with transitions of the type $S_z \rightleftharpoons S_z - 1$ have been indicated by S_z . In the spectrum for $\text{CaF}_2:\text{Gd}^{3+}, \text{Li}^+$ we distinguish between two signals: first, the signal due to complexes which are oriented perpendicular to the magnetic field direction; the EPR lines of this signal have been indicated by boxed S_z 's. Second, there is a signal due to 45° complexes.

III. EXPERIMENTAL RESULTS

A. CaF_2

In CaF_2 doped with small amounts of GdF_3 one usually observes different types of EPR spectra. First, there is a cubic signal consisting of seven lines; this spectrum has been described by Low²¹ and Rytter.²² In crystals which are prepared with

care such that oxygen and hydroxyl ions are prevented from entering the material, one finds EPR signals due to complexes resulting from charge compensation with interstitial fluorine ions. These signals have been described by Franklin and Marzullo.⁴

In order to produce charge compensation centers of the type $\text{Gd}^{3+}-M^+$ in CaF_2 we have to get rid of the gadolinium-interstitial F^- complexes. This has been achieved by the method suggested by Miner *et al.*⁵ and Vlasova *et al.*²³; apart from Gd^{3+} and M^+ we introduced 500–600-ppm Ce^{3+} into the crystal. In these crystals we observe a signal due to cubic Gd^{3+} (see Fig. 2, upper curve) and another EPR spectrum associated with $\text{Gd}^{3+}-M^+$ complexes (Fig. 2, lower curve). The intensity of the signal due to gadolinium-interstitial F^- complexes has been reduced by at least a factor of 100.

We have investigated $\text{Gd}^{3+}-M^+$ complexes in CaF_2 , where M^+ is Li^+ , Na^+ , K^+ , Rb^+ , Cs^+ , and Ag^+ . Experiments on crystals doped with Cu^+ , Au^+ , Hg^+ , and Tl^+ were unsuccessful. A general feature of our experimental results for $\text{Gd}^{3+}-M^+$ complexes in CaF_2 is that the overall splitting of the spectrum increases with increasing M^+ radius. We have also observed that the intensity of the signals due to the $\text{Gd}^{3+}-M^+$ complexes decreases with increasing M^+ radius, indicating that either the solubility of MF in CaF_2 decreases with increasing M^+ radius or the association energy of $\text{Gd}^{3+}-M^+$ complexes decreases with increasing M^+ radius.

As an example we show in Fig. 3 a rotational diagram obtained for $\text{CaF}_2:\text{Gd}^{3+}, \text{Li}^+$; the axis of rotation is the $[100]$ axis. The maximum overall splitting is found for $\vec{H}_0 \parallel [100]$. The interpretation

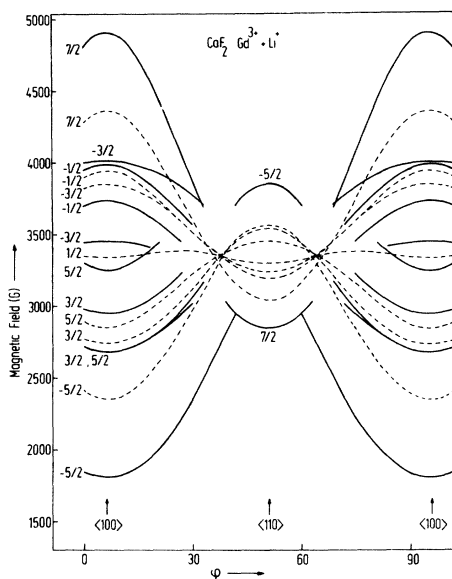


FIG. 3. Rotational diagram of the EPR lines observed in $\text{CaF}_2:\text{Gd}^{3+}, \text{Li}^+$. The axis of rotation is $[100]$. The broken curves are associated with transitions of cubic Gd^{3+} ; the drawn lines correspond with transitions of the $\text{Gd}^{3+}-\text{Li}^+$ complexes with C_{2v} symmetry. The curves indicated by S_z are due to transitions of the type $S_z \rightleftharpoons S_z - 1$.

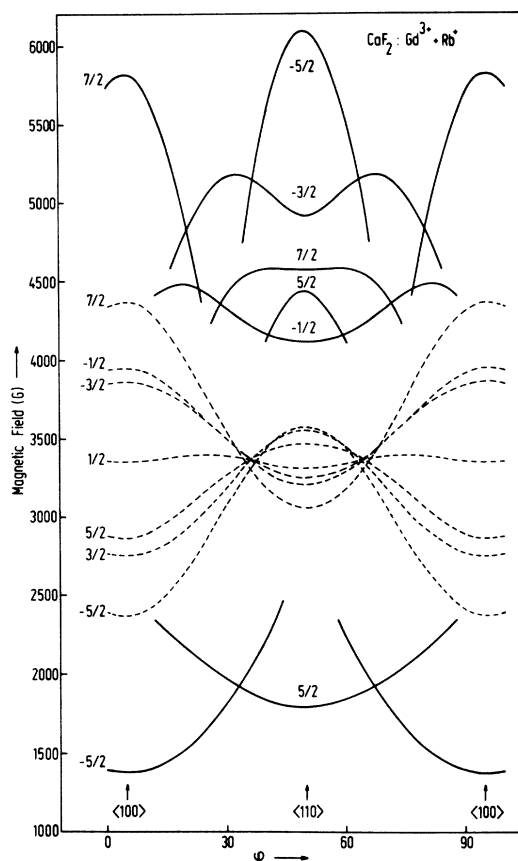


FIG. 4. Rotational diagram of the EPR lines observed in $CaF_2:Gd^{3+}, Rb^+$; the axis of rotation is $[100]$. The broken lines are associated with transitions of cubic Gd^{3+} , the drawn lines correspond with C_{2v} symmetry centers. The curves indicated by S_z are due to transitions of the type $S_z \pm 1$.

of the various lines has been found by using the method described by Bijvank and den Hartog.¹⁹ We can associate the EPR lines due to $Gd^{3+}-M^+$ complexes with definite excitations of the type $S_z \rightarrow S_z + 1$ because the corresponding EPR lines of the cubic spectrum have been designated; i.e., the signs of the cubic crystal-field parameters are known.²⁴

In Fig. 4 we have plotted the rotational behavior of the EPR lines found in $CaF_2:Gd^{3+}, Rb^+$ and which could be associated with cubic Gd^{3+} or $Gd^{3+}-Rb^+$ complexes. The low-field part of the spectra was obscured by forbidden transitions, which have rather large intensities because we are dealing with large crystal fields. It can be seen from Fig. 4 that for $Gd^{3+}-Rb^+$ complexes the overall splitting is larger for $\vec{H}_0 \parallel [110]$ than for $\vec{H}_0 \parallel [100]$. We note that on going from Li^+ to Cs^+ the extra splitting for the $-\frac{5}{2} \approx -\frac{7}{2}$ transition of $Gd^{3+}-M^+$ increases from 280 G to an estimated value of 4000 G.

In order to interpret the results obtained for the $Gd^{3+}-M^+$ complexes in CaF_2 we have first determined the crystal-field parameters B_4^0 , B_4^4 , B_6^0 , and B_6^4 of the spin Hamiltonian corresponding with cubic Gd^{3+} in CaF_2 . The least-squares fits to the rotational diagrams agreed with the experimental curves within error bars of 1.5 G. Also our values for the crystal-field parameters agree well with those reported in the literature.^{21,22,24} In the above-mentioned situation the principal axes x , y , and z were chosen along the crystallographic $\langle 100 \rangle$ directions. In case of orthorhombic $Gd^{3+}-M^+$ complexes it is convenient to choose the principal z axis along $[110]$. The new set of principal axes have been indicated in Fig. 1. This implies that one has to rotate the frame of axes and the crystal-field parameters will change correspondingly.

In Table I we have compiled the experimental results obtained for the $Gd^{3+}-M^+$ complexes observed in CaF_2 . As a reference we have given the crystal-field parameters of cubic Gd^{3+} with respect to the new frame of axes. Because we are mainly interested in the changes of the crystal-field parameters due to the presence of the excess charge of the substitutional M^+ ions, we have compiled in Table I the changes of these parameters as compared to the parameters of cubic Gd^{3+} .

In a few cases some of the parameters could not be determined with reasonable accuracy. Sometimes this was due to the small extra crystal-field splitting; in other cases the signal-to-noise ratio was the reason. It should be noted here, that the

TABLE I. Spin-Hamiltonian parameters B_n^m for orthorhombic complexes $Gd^{3+}-M^+$ in CaF_2 .

M	B_2^0 (± 0.2 G)	B_2^2 (± 0.2 G)	B_4^0 (± 0.005 G)	B_4^4 (± 0.05 G)	B_4^4 (± 0.05 G)	B_6^0 ($\pm 5 \times 10^{-4}$ G)
cubic	0	0	0.209	4.19	-3.14	1.5×10^{-4}
Li	14.9	-49.1	-0.015	-0.34	-0.09	...
Na	13.2	-20.3	0	-0.25	-0.12	-2.4×10^{-4}
K	83.6	-20.1	-0.024	-0.22	-0.13	-0.2×10^{-4}
Rb	141.8	-11.9	-0.028	-0.25	-0.10	0.7×10^{-4}
Cs	220.5	-4.0	-0.040	-0.46	-0.11	0.3×10^{-4}
Ag	50.9	-26.3	-0.024	-0.34	-0.20	2.7×10^{-4}

TABLE II. Spin-Hamiltonian parameters B_i^m for orthorhombic complexes $Gd^{3+}-M^+$ in CaF_2 , according to the alternative interpretation of the spectra with $\vec{H}_0 \parallel [110]$ (see text).

M	B_2^0 (± 0.2 G)	B_2^2 (± 0.2 G)	B_4^0 (± 0.005 G)	B_4^2 (± 0.05 G)	B_4^4 (± 0.05 G)	B_6^0 ($\pm 5 \times 10^{-4}$ G)
cubic	0	0	0.209	4.19	-3.14	1.5×10^{-4}
Li	17.7	-46.3	-0.070	-0.12	0.29	...
Na	3.4	-30.0	-0.045	-0.07	0.19	-3.5×10^{-4}
K	-31.8	-135.5	-0.052	-0.11	0.08	2.4×10^{-4}
Rb	-65.0	-218.7	-0.054	-0.15	0.08	-4.9×10^{-4}
Cs	-108.3	-332.5	-0.084	-0.28	0.20	-0.8×10^{-4}
Ag	-12.3	-89.6	-0.075	-0.13	0.17	-3.0×10^{-4}

crystal-field parameters found for $CaF_2:Gd^{3+}$, Ag^+ fit nicely into the series $CaF_2:Gd^{3+}$, $Li^+-CaF_2:Gd^{3+}$, Cs^+ . We therefore assume that, when introduced into CaF_2 , silver becomes monovalent.

As discussed earlier¹⁹ the determination of the crystal-field parameters is not ambiguous because of the fact that we cannot distinguish between perpendicular and parallel complexes when $\vec{H}_0 \parallel [110]$. This leads to an alternative interpretation of the observed spectra and consequently to an alternative table of crystal-field parameters given in Table II.

B. BaF_2

When small concentrations (100–200 ppm) of Gd^{3+} are introduced into BaF_2 one mainly observes an EPR signal which shows trigonal symmetry. When measured with $\vec{H}_0 \parallel [100]$ the signal is very similar to the one of cubic Gd^{3+} in BaF_2 . Increasing the concentration of Gd^{3+} leads to very complex EPR spectra which have not been studied in detail. In samples doped with small amounts of Gd^{3+} and M^+ one observes mainly cubic Gd^{3+} and also orthorhombic $Gd^{3+}-M^+$ complexes. When sufficient concentrations (1000–1500 ppm) of M^+ ions are present the trigonal EPR signals have disappeared completely.

It appeared that the solubility of LiF in BaF_2 is very low; when 1500-ppm LiF is added to the BaF_2 raw material before crystal growth the resulting crystals have a milky appearance. The EPR signals were predominantly due to trigonal centers; charge compensation centers of the type

$Gd^{3+}-Li^+$ have not been observed.

Crystals doped with silver or copper fluoride were colored yellow and red, respectively. In addition we found small metallic crystallites at the surface of the BaF_2 boule. Using an optical transmission microscope we found that inside the crystal small metallic precipitates are present. Probably the coloration of the crystals is due to absorption by small metallic particles. Similar absorptions have been found in additively colored alkali halides and alkaline-earth fluorides.^{25–29}

In BaF_2 crystals doped with AgF or CuF and GdF_3 we have not detected signals due to orthorhombic complexes. Like in the case of $BaF_2:Gd^{3+}$, Li^+ we have to conclude here that the solubility of Ag^+ or Ag^0 and Cu^+ or Cu^0 is very low. The EPR spectra observed in these crystals are again due to centers of trigonal symmetry.

In BaF_2 we have investigated orthorhombic defects of the type $Gd^{3+}-Na^+$, $Gd^{3+}-K^+$, $Gd^{3+}-Rb^+$, and $Gd^{3+}-Cs^+$. The overall splittings of these spectra are appreciably smaller than in CaF_2 . The general trend of the splitting however is the same as for CaF_2 .

The crystal-field parameters for the above-mentioned complexes as determined from the rotational diagrams have been compiled in Tables III and IV.

C. $SrCl_2$

The experimental results presented in an earlier paper¹⁹ have been reinterpreted on the basis of the Hamiltonian (1), which contains fourth- and

TABLE III. Spin-Hamiltonian parameters B_i^m for orthorhombic complexes $Gd^{3+}-M^+$ in BaF_2 .

M	B_2^0 (± 0.2 G)	B_2^2 (± 0.2 G)	B_4^0 (± 0.005 G)	B_4^2 (± 0.05 G)	B_4^4 (± 0.05 G)	B_6^0 ($\pm 5 \times 10^{-4}$ G)
cubic	0	0	0.161	3.23	-2.42	1.5×10^{-4}
Na	-7.6	-74.2	-0.029	-0.13	-0.04	-5.5×10^{-4}
K	-14.1	-53.6	-0.019	-0.08	-0.02	1.0×10^{-4}
Rb	1.9	-57.2	-0.038	-0.21	-0.10	-16.3×10^{-4}
Cs	33.3	-65.9

TABLE IV. Spin-Hamiltonian parameters B_i^n for orthorhombic complexes $Gd^{3+}-M^+$ in BaF_2 , according to the alternative interpretation of the spectra with $\vec{H}_0 \parallel [110]$ (see text).

M	B_2^0 (± 0.2 G)	B_2^2 (± 0.2 G)	B_4^0 (± 0.005 G)	B_4^2 (± 0.05 G)	B_4^4 (± 0.05 G)	B_6^0 ($\pm 5 \times 10^{-4}$ G)
cubic	0	0	0.161	3.23	-2.42	1.5×10^{-4}
Na	40.9	-25.6	-0.031	-0.12	-0.03	2.0×10^{-4}
K	33.9	-5.7	-0.018	-0.08	-0.02	0.2×10^{-4}
Rb	27.7	-31.5	-0.052	-0.15	-0.01	22.7×10^{-4}
Cs	16.3	-83.0

sixth-degree terms. Here too, we have the problem that the determination of the crystal-field parameters is ambiguous. These parameters are given in Tables V and VI. In contrast with the results obtained for CaF_2 and BaF_2 we have not observed centers produced by local charge compensation in $SrCl_2:Gd^{3+}$ (i.e., without additional M^+ impurities).

We have studied the temperature dependence of the various EPR signals observed in $SrCl_2:Gd^{3+}, M^+$. The variations of the cubic signal as a function of temperature have been shown in Fig. 5. We have plotted the changes of the line positions as compared to those observed at $-150^\circ C$. The total relative change of the overall splitting amounts to 10%. This change is larger than expected when simple lattice expansion as a function of temperature is taken into account. Between -150 and $50^\circ C$ the lattice parameter was found to change 0.5%. This implies that the fourth-degree crystal-field parameter changes by about 2.5%. It was found by Huang³⁰ that normal vibrations also contribute to the crystal-field splitting. According to the calculations of this author for $CaF_2:Gd^{3+}$ the vibrational contribution at 293 K can be as large as 25%. The estimated zero-point phonon contribution amounts to about 14%; thus the change of the observed crystal-field splitting of approximately 10% seems to be reasonable.

For orthorhombic centers of the type $Gd^{3+}-Li^+$ the variations of the extra crystal-field splitting as a function of temperature (see Fig. 6) agree well with the values expected on the basis of a simple expansion of the polarizable point-ion system as will be shown in Sec. IV. From the shapes of the curves given in Figs. 5 and 6 we see that below LN_2 temperature the changes of the crystal-field parameters will be very small. In addition we conclude that the vibrational contribution to the second-degree crystal-field parameters is, in contrast with the cubic situation, negligibly small.

IV. THEORY

A. Crystal-field splitting

The behavior of the EPR lines of trivalent gadolinium ions in orthorhombic symmetry can be described by the spin Hamiltonian (1). We note that in this Hamiltonian even terms are present; odd terms do not contribute because these terms are not invariant with respect to time reversal. In general, however, the crystal field of orthorhombic symmetry can be described by the following formula:

$$V_c = c_0^0 + c_1^0 P_1^0 + c_2^0 P_2^0 + c_2^2 P_2^2 + c_3^0 P_3^0 + c_3^2 P_3^2 + c_4^0 P_4^0 + \dots, \quad (2)$$

where P_i^n are the homogeneous polynomials as

TABLE V. Spin-Hamiltonian parameters B_i^n for orthorhombic complexes $Gd^{3+}-M^+$ in $SrCl_2$.

M	B_2^0 (± 0.2 G)	B_2^2 (± 0.2 G)	B_4^0 (± 0.005 G)	B_4^2 (± 0.05 G)	B_4^4 (± 0.05 G)	B_6^0 ($\pm 5 \times 10^{-4}$ G)
cubic	0	0	0.068	1.33	-1.02	0.3×10^{-4}
Li	-29.0	-87.9	0.001	-0.18	-0.04	2.4×10^{-4}
Na	-24.9	-60.0	0.002	-0.11	-0.02	0.3×10^{-4}
K	-11.4	-52.1	0.010	-0.14	-0.07	-0.7×10^{-4}
Rb	-1.5	-51.3	0.013	-0.14	-0.12	-2.0×10^{-4}
Cs	13.8	-45.9	0.056	-0.63	-1.04	...
Ag	-29.9	-75.8	0.007	-0.12	-0.06	-0.8×10^{-4}
Cu	-36.7	-100.8
Tl	-0.4	-56.3
Ba	12.9	2.2	-0.118	-0.20	0.16	...
Ca	2.2	-2.2

TABLE VI. Spin-Hamiltonian parameters B_i^m for orthorhombic complexes $\text{Gd}^{3+}-M^+$ in SrCl_2 , according to the alternative interpretation of the spectra with $\vec{H}_0 \parallel [110]$ (see text).

M	B_2^0 (± 0.2 G)	B_2^2 (± 0.2 G)	B_4^0 (± 0.005 G)	B_4^2 (± 0.05 G)	B_4^4 (± 0.05 G)	B_6^0 ($\pm 5 \times 10^{-4}$ G)
cubic	0	0	0.068	1.33	-1.02	0.3×10^{-4}
Li	58.4	-0.4	-0.031	-0.06	0.17	0.9×10^{-4}
Na	42.4	7.3	-0.020	-0.03	0.13	0.9×10^{-4}
K	31.8	-8.9	-0.025	0.00	0.18	0.2×10^{-4}
Rb	26.4	-23.3	-0.030	0.04	0.19	0.1×10^{-4}
Cs	16.1	-43.7	-0.191	0.36	0.69	...
Ag	52.8	6.9	-0.024	0.00	0.15	0.7×10^{-4}
Cu	68.8	4.7
Tl	28.4	-27.6
Ba	-7.6	-18.3	-0.053	-0.47	-0.30	...
Ca	0	-4.4

defined by Abragam and Bleaney.⁸ For convenience we give c_0^0 , c_1^0 , c_2^0 , and c_2^2 in terms of the point-ion-lattice model:

$$\begin{aligned}
 c_0^0 &= \frac{1}{4\pi\epsilon_0} \sum_j \frac{q_j}{R_j}, \\
 c_1^0 &= \frac{1}{4\pi\epsilon_0} \sum_j \frac{q_j Z_j}{R_j^3}, \\
 c_2^0 &= \frac{1}{16\pi\epsilon_0} \sum_j \frac{q_j (3Z_j^2 - R_j^2)}{R_j^5}, \\
 c_2^2 &= \frac{3}{16\pi\epsilon_0} \sum_j \frac{q_j (X_j^2 - Y_j^2)}{R_j^5}.
 \end{aligned} \quad (3)$$

Here, q_j is the charge of the j th ion; X_j , Y_j , Z_j , and R_j correspond with the position coordinates of ion j . Induced-point dipoles also contribute to the crystal-field parameters. Formulas similar to those in (3) can easily be derived.

Although the odd terms $c_1^0 P_1^0$, $c_3^0 P_3^0$, and $c_3^2 P_3^2$ do not directly contribute to the splitting of the energy levels, it has been shown by Kiel³¹ that in second order these odd terms give rise to even contribu-

tions to the spin Hamiltonian. These contributions are called equivalent even fields.

In this paper we shall use two mechanisms to obtain the second-degree parameters of the spin Hamiltonian from the electrostatic crystal-field potential. The first mechanism was introduced by Hutchison, Judd, and Pope⁹:

$$B_2^0 = \frac{4}{5} (\xi^3 / W_P^2 W_D) \gamma_2 e \langle r^2 \rangle c_2^0. \quad (4)$$

Here, ξ is the one-electron spin-orbit coupling parameter; W_P and W_D are the energy separations between the ground state $^8S_{7/2}$ and the excited states denoted by $^6P_{7/2}$ and $^6D_{7/2}$, respectively; γ_2 is the screening factor; and $\langle r^2 \rangle$ is the average of the operator r^2 for a $4f$ electron of Gd^{3+} . When the values of the ionic constants are used we find that $B_2^0 = 4.38 \times 10^{-16} c_2^0$ G (c_2^0 is given in V/m^2).

The second mechanism was proposed by Wybourne.¹⁰ According to this mechanism the relation between c_2^0 and B_2^0 is given by

$$B_2^0 = - \frac{16}{735} \gamma_2 e c_2^0 \xi (-5R_{++}^2 + 3R_{+-}^2 + 2R_{--}^2) / W_P. \quad (5)$$

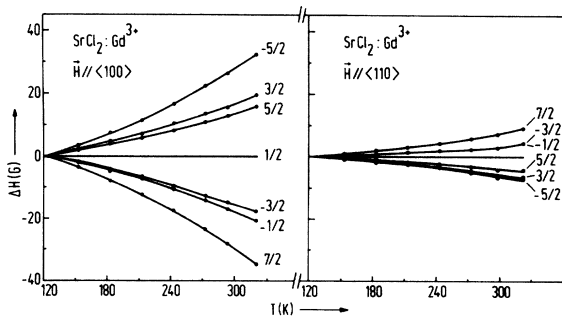


FIG. 5. Temperature dependence of the cubic EPR lines of $\text{SrCl}_2:\text{Gd}^{3+}$ for two directions of the magnetic field. The shifts of the various lines with respect to the position at 120 K have been given.

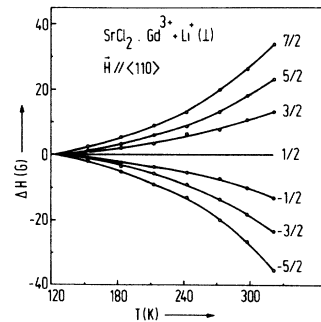


FIG. 6. Temperature dependence of the orthorhombic EPR lines in $\text{SrCl}_2:\text{Gd}^{3+}, \text{Li}^+$ for $\vec{H} \parallel [110]$. Here we have selected the signals due to perpendicular complexes. The shifts of the various lines with respect to the position at 120 K have been given.

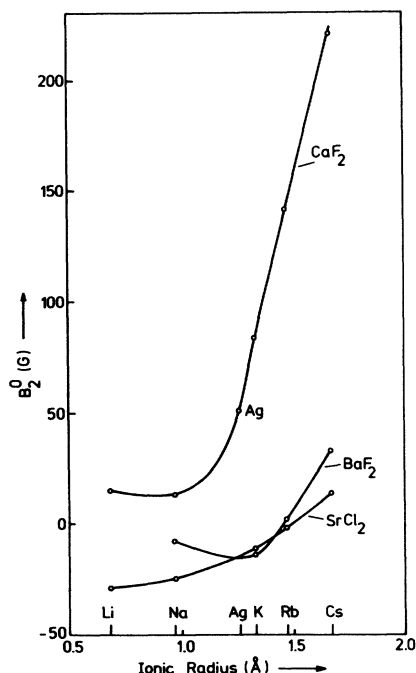


FIG. 7. Behavior of the crystal-field parameter B_2^0 as a function of the ionic radius of the additional monovalent metal impurity.

Here, R_{++} , R_{+-} , and R_{--} are the relativistic integrals calculated by Waber and Cromer.³² The contribution from this mechanism is $B_2^0 = 5.82 \times 10^{-18} c_2^0$ G. In accordance with the Wigner-Eckart theorem, $B_2^0/c_2^0 = B_2^2/c_2^2$, thus for B_2^2 relations similar to (4) and (5) can be given.

The second-order effect of odd crystal fields has been given by formula (6) in Kiel's paper; this formula, however, should be corrected by a factor $1/\pi$. We have evaluated the contributions due to terms containing $(c_1^0)^2$, $c_1^0 c_3^0$, $(c_3^0)^2$, $c_3^0 c_1^0$, and $c_3^0 c_3^0$; it was found that the term with $(c_1^0)^2$ is dominant. It turns out that $(c_2^0)_{eq} = 2.71 \times 10^{-2} (c_1^0)^2$, where the subscript eq stands for equivalent. It should be noted that $(c_2^0)_{eq}$ can be connected with $(B_2^0)_{eq}$ by using (4). This gives us

$$B_2^0 = 1.19 \times 10^{-19} (c_1^0)^2 \text{ G.} \quad (6)$$

The second-order contributions of odd crystal-field terms to B_2^2 were found to be zero $[(c_1^0)^2, c_1^0 c_3^0, \text{ and } (c_3^0)^2]$ or negligible $(c_3^0 c_1^0 \text{ and } c_3^0 c_3^0)$.

Finally we have contributions due to second-order effects as given by the relativistic treatment due to Parrot.³³ In the present paper we have applied formulas similar to those given by Parrot³³ and de Beer *et al.*³⁴ For the relativistic integrals and energy differences necessary to calculate the relativistic equivalent even fields we have used the values calculated by Andriessen.³⁵ In the pres-

ent calculations we have taken into account contributions due to discrete as well as continuum states. The result is

$$B_2^0 = 3.41 \times 10^{-19} (c_1^0)^2 \text{ G.}$$

Taking into account all contributions discussed above we find that

$$(B_2^0)_{tot} = 10.20 \times 10^{-18} c_2^0 + 4.60 \times 10^{-19} (c_1^0)^2, \quad (8)$$

where the subscript tot stands for total. For B_2^2 we can write approximately

$$B_2^2 = 10.20 \times 10^{-18} c_2^2. \quad (9)$$

B. Electrostatic model

As mentioned in an earlier paper, the interesting feature of the complexes studied here is that to a high degree of approximation we only need to consider contributions to the crystal field due to ions immediately neighboring the defect. The major contributions to the extra crystal-field splittings come from the electrostatic interaction between the $4f^7$ electron system and the surrounding monopoles, the induced electronic dipoles and distortion effects. The latter effect will give increased contributions as the radius of the compensating impurity increases. This can be seen from Figs. 7 and 8, where B_2^0 and B_2^2 as a function of the ionic radius of the impurity have been given.

We first consider the excess negative charge of the monovalent impurity, which contributes to c_1^0 and c_2^0 (we chose the principal z axis along the line connecting Gd^{3+} and M^+). This contribution does not give rise to a term of the type $B_2^2 O_2^2$ in the spin Hamiltonian implying that the other con-

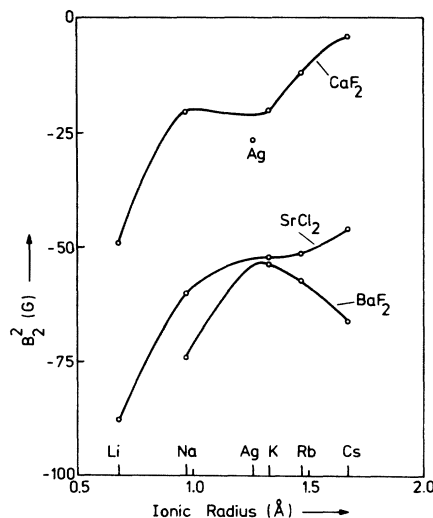


FIG. 8. Behavior of B_2^2 as a function of the radii of the additional impurities.

TABLE VII. Computed shifts of the type-I halide ions along the \tilde{x} and \tilde{z} directions for complexes in SrCl_2 , CaF_2 , and BaF_2 .

<i>M</i>	SrCl_2		CaF_2		BaF_2	
	Δx (Å)	Δz (Å)	Δx (Å)	Δz (Å)	Δx (Å)	Δz (Å)
Li	0.000	-0.020	0.035	0.063
Na	-0.005	0.025	0.025	0.080	0.055	-0.005
K	0.015	0.037	0.080	0.087	0.045	0.020
Rb	0.035	0.040	0.123	0.097	0.067	0.017
Cs	0.065	0.045	0.180	0.107	0.115	0.010
Ag	-0.020	0.110	0.055	0.080
Ba	0.000	-0.027

tributions are significant. The dipoles induced by the excess negative charge predominantly contribute to $B_2^0 O_2^0$; the effect on c_1^0 and c_2^0 is small. As expected, we have found that the displacements of the halide ions of type I in Fig. 1 give the major contributions to the extra crystal-field splitting. The effect on c_1^0 turns out to be rather small, but depending upon the direction in which the displacement takes place, significant effects have been observed on the parameters c_2^0 and c_2^2 .

When the effects indicated above and discussed in Sec. IV A are taken into account we can fit the theoretical values of the second-degree crystal-field parameters B_2^0 and B_2^2 to the experimentally observed values given in Tables I–VI. Here we have used for the polarizability $0.85 \times 10^{-24} \text{ cm}^3$ and $2 \times 10^{-24} \text{ cm}^3$ for F^- and Cl^- respectively. From these fits we obtain values for the shifts of the type-I halide ions along the x and z direction. The shift along the y direction is 0; this can be seen from the symmetry of the complexes. The fitted displacements for the systems $\text{SrCl}_2:\text{Gd}^{3+}, M^+$, $\text{CaF}_2:\text{Gd}^{3+}, M^+$, and $\text{BaF}_2:\text{Gd}^{3+}, M^+$ have been given in Table VII. The values given in Table VII correspond with the extra crystal-field parameters given in Tables I, III, and V. The alternative interpretation of the EPR spectra leading to the

TABLE VIII. Computed shifts of the type-I halide ions along the \tilde{x} and \tilde{z} directions for complexes in SrCl_2 , CaF_2 , and BaF_2 , according to the alternative interpretation of the spectra with $\tilde{H}_0 \parallel [110]$ (see text).

<i>M</i>	SrCl_2		CaF_2		BaF_2	
	Δx (Å)	Δz (Å)	Δx (Å)	Δz (Å)	Δx (Å)	Δz (Å)
Li	0.110	0.140	0.035	0.060
Na	0.075	0.150	0.020	0.073	0.115	0.060
K	0.070	0.120	0.015	0.005	0.097	0.085
Rb	0.070	0.090	0.000	-0.043	0.100	0.050
Cs	0.063	0.050	-0.030	-0.100	0.095	-0.010
Ag	0.135	0.285	0.020	0.037
Ba	0.015	0.005

crystal-field parameters given in Tables II, IV, and VI gives rise to fitted displacements as given in Table VIII.

We emphasize that in SrCl_2 we have to assume that Ag and Cu are present in the atomic state. Therefore, they should be treated as double negative charges. Ca and Ba, however, have the same valency as Sr and should therefore be treated as zero charges with respect to the crystal lattice.

V. DISCUSSION

The positions of the type-I fluorine ions as compiled in Table VII for $\text{CaF}_2:\text{Gd}^{3+}, M^+$ have been depicted in Fig. 9. From this figure we see that for small M^+ ions, the type-I fluorines have shifted predominantly along the z direction. When the size of the compensating impurity increases the displacement direction is almost parallel to the x direction.

It was shown in the previous sections that, in principle, there is another set of displacements which has been plotted in Fig. 10. Here, we see that for large M^+ ions the main component of the shift is parallel to the z direction.

The two possibilities discussed above equally

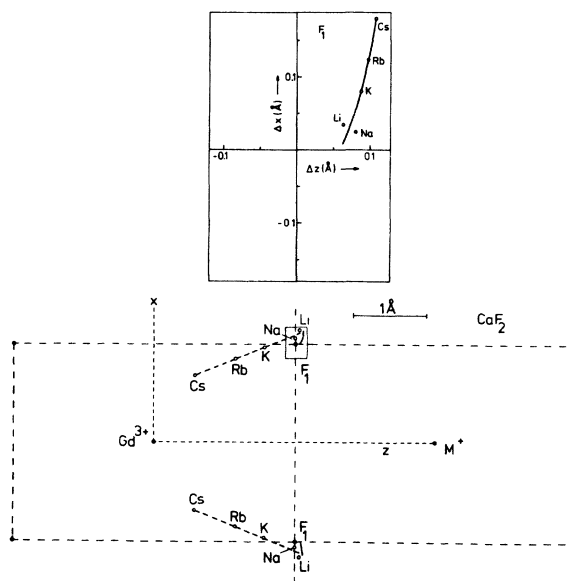


FIG. 9. Two-dimensional representation of an orthorhombic $\text{Gd}^{3+}-M^+$ complex; only the nearest neighbors of the impurity ions located in the x, z plane have been given. The shift of the F_1 ions for $\text{Gd}^{3+}-M^+$ complexes in CaF_2 as calculated using the point charge model and the superposition model have been shown. The shift of the F_1 ions, indicated by the drawn line corresponds with the point charge model; it has been given enlarged in the upper figure. The positions of the F_1 ions for the various complexes as shown in the lower figure correspond with the superposition model.

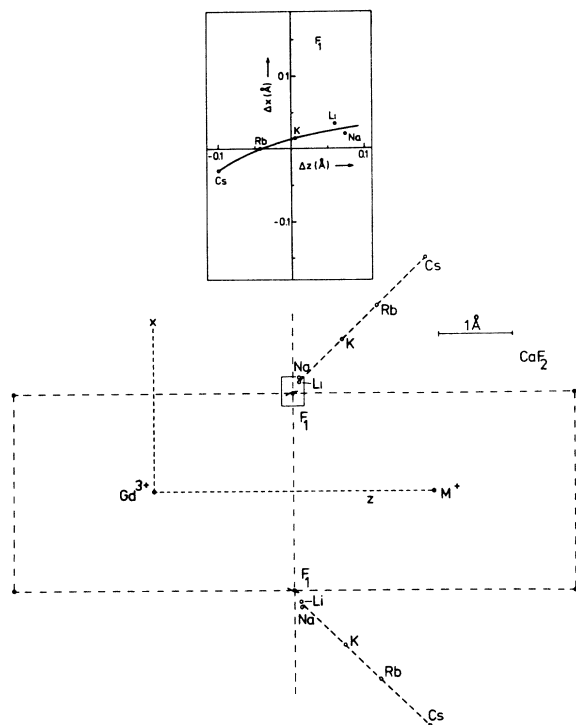


FIG. 10. Two-dimensional representation of an orthorhombic Gd^{3+} - M^+ complex. The shift of the F_1 ions for Gd^{3+} - M^+ complexes in CaF_2 as calculated by using the point-charge model and the superposition model have been shown. For the calculations we have assumed here that the alternative interpretation of the spectra for $\vec{H} \parallel [110]$ is correct. The shift of the F_1 ions, indicated by the drawn line within the box of the lower figure, has been given enlarged in the upper figure; it corresponds with the point charge model. The positions of the F_1 ions for the various complexes as shown in the lower figure correspond with the superposition model.

well describe the observed behavior of the EPR spectra. From a physical point of view the second set of displacements is less attractive. It is hard to believe that the distance between the Gd^{3+} impurity and the type-I F^- ions becomes smaller than for Gd^{3+} in a cubic environment. We expect that with increasing ionic M^+ radius the type-I F^- ions are pushed in outward directions. This expectation agrees with the results shown in Fig. 9. The results for $SrCl_2$ and BaF_2 are of similar nature; here too, we distinguish between two possibilities. For one of them the displacement of the type-I halide ions is directed towards the Gd^{3+} impurity. In the alternative case the shift is directed mainly along \vec{x} . The magnitude of the shift is expected to be smaller than the difference between the ionic radius of the host crystal ion and that of the M^+ impurity. For $CaF_2:Gd^{3+}$, Cs the difference is 0.55 Å and the calculated shift is 0.21 Å. From

this we conclude that both the direction and magnitude of the shift of F^- ions are acceptable.

The temperature-dependent experiments on Gd^{3+} - M^+ complexes in $SrCl_2$ indicate that the variations of the second-degree crystal-field parameters are due to expansion of the lattice. Furthermore, no important phonon contributions are present, indicating that the theoretical treatment given in Sec. IV is sufficient.

We shall now discuss our experimental results for complexes in CaF_2 in terms of the superposition model proposed by Newman and Urban.¹⁷ These authors suggest that the crystal-field parameters describing the fine splitting of Gd^{3+} are determined by the nature and position of the ligands directly surrounding this magnetic impurity. The main contributions are supposed to be not electrostatic but due to overlap and covalency effects.

In accordance with Newman and Urban¹⁷ we write that a single ligand centered on an open shell ion gives the following contribution to the second-degree crystal-field parameters:

$$K_2^m(\theta, \phi) \bar{A}_2(R). \quad (10)$$

In this expression the intrinsic parameter $\bar{A}_2(R)$ is the axially symmetric crystal field due to a single ligand at distance R from the center of the Gd^{3+} ion. The factors $K_2^m(\theta, \phi)$ are given by

$$\begin{aligned} K_2^0(\theta, \phi) &= \frac{1}{2}(3 \cos^2 \theta - 1), \\ K_2^2(\theta, \phi) &= \frac{3}{2} \sin^2 \theta \cos 2\phi. \end{aligned} \quad (11)$$

The function $\bar{A}_2(R)$ can be given by

$$\bar{A}_2(R) = \bar{A}_2(R_0) (R_0/R)^t, \quad (12)$$

where $t=7$, and R_0 is the unperturbed interionic distance. Since the parameter $\bar{A}_2(R)$ is connected with the intrinsic parameter $\bar{B}_2(R)$ (see Newman and Urban¹⁷) we can write

$$\bar{B}_2(R) = \bar{B}_2(R_0) (R_0/R)^{t'}. \quad (13)$$

Newman and Urban find for t' associated with interactions with F^- an average value of -1 ; for $\bar{B}_2(R_0)$ we have taken the same value as used by Edgar and Newman¹⁸ for $CaF_2:Gd^{3+}$, Na^+ [$\bar{B}_2(R_0) = \frac{1}{3} \bar{b}_2(R_0) = -231$ G].

For a perfectly cubic coordination the sum of the contributions to the spin-Hamiltonian parameters B_2^0 and B_2^2 from the first coordination shell will be zero. In order to obtain a net effect due to the ligands directly surrounding the Gd^{3+} ion we have to introduce distortions. (Note that in accordance with Edgar and Newman¹⁸ the effect of the effective negative charge of the M^+ ion has not been taken into account.) For B_2^0 we may write

$$B_2^0 = \sum_{i=1}^8 \frac{3 \cos^2 \theta_i - 1}{2} \bar{B}_2(R_0) \left(\frac{R_0}{R_i} \right)^{t'}, \quad (14)$$

TABLE IX. Computed shifts of the type-I halide ions along the \tilde{x} and \tilde{z} directions for complexes in CaF_2 according to the superposition model. The right-hand columns refer to the alternative interpretation of the spectra with $\tilde{H}_0 \parallel [110]$ (see text).

M	CaF_2		CaF_2	
	$\Delta x(\text{\AA})$	$\Delta z(\text{\AA})$	$\Delta x(\text{\AA})$	$\Delta z(\text{\AA})$
Li	0.208	0.065	0.222	0.086
Na	0.080	-0.007	0.146	0.087
K	-0.052	-0.435	0.737	0.676
Rb	-0.210	-0.825	1.212	1.173
Cs	-0.430	-1.372	1.856	1.839
Ag	0.042	-0.214	0.473	0.395

while for B_2^0 we find a similar relationship. Here, θ_i and R_i are polar coordinates of the ions surrounding the Gd^{3+} ion; for the direction $\theta=0$ we have chosen the z direction of the complex (see Fig. 1).

Applying (14) to the system $\text{CaF}_2:\text{Gd}^{3+}, \text{Na}^+$ we find excellent agreement between our calculated values for the distortions and those obtained by Edgar and Newman.¹⁸ Analogous to the distortions calculated on the basis of the point ion lattice model (see Sec. IV) we have obtained shifts of the type-I fluoride ions in the (110) plane. Because spectroscopically one cannot distinguish between the two alternative interpretations indicated above, we obtain two sets of calculated shifts, which have been compiled in Table IX.

We note that in general the shifts given in Table IX are one order of magnitude larger than those given in Tables VII and VIII. The total shifts obtained for the complex $\text{Gd}^{3+}-\text{Cs}^+$ are 1.44 and 2.61 \AA for the two alternative interpretations. It is immediately clear that shifts of this magnitude are completely unrealistic. In order to demonstrate the difference between the distortions obtained on the basis of the electrostatic model (Sec. IV) and the superposition model we have depicted the shifts for the various complexes in CaF_2 in Figs. 9 and 10.

It is now of interest to investigate more closely the reasons for the deviating results of the two

models. From the treatment given in Sec. IV it is easy to see that the contributions to the second-degree crystal-field parameters vary as $1/R^3$ when interactions with monopoles are considered, and as $1/R^6$ when one takes into account contributions from induced dipoles. From the treatment of the superposition model we observe that the second-degree crystal-field parameters are proportional to R . This leads to slow variations of B_2^0 and B_2^2 as a function of the interionic distance, and consequently large distortions are necessary to explain the observed extra crystal-field splittings.

Another difference between the model employed in the present paper and the superposition model is that in the former model the second-order contribution from odd crystal-field terms are included, whereas in the superposition model this is not the case. We have found that for the complexes studied here this is not too important because the total contribution due to this effect is about 20%. We emphasize that for low-symmetry systems the second-order effect of odd terms may become very important especially when one deals with small values of B_2^0 .

The shifts compiled in Tables VII and VIII should be observable by means of electron-nuclear-double-resonance experiments, which will give an accurate test to distinguish between the two alternative interpretations of the spectra. Also these experiments, which are contemplated, will provide a possibility to assess the merits of the dielectric interaction model employed in this paper.

ACKNOWLEDGMENTS

The authors wish to thank P. Wesseling for growing the crystals. We are grateful to Dr. R. de Beer and Dr. D. van Ormondt of the Technical University of Delft for stimulating discussions. This work is part of the research program of the "Stichting voor Fundamenteel Onderzoek der Materie" (F.O.M.) and has been made possible by financial support from the "Nederlandse Organisatie voor Zuiver Wetenschappelijk Onderzoek" (Z.W.O.).

¹E. L. Kitts, Jr., M. Ikeya, and J. H. Crawford, Jr., Phys. Rev. B **8**, 5840 (1973).

²B. P. M. Lenting, J. A. J. Numan, E. J. Bijvank, and H. W. den Hartog, Phys. Rev. B **14**, 1811 (1976).

³W. van Weperen, B. P. M. Lenting, E. J. Bijvank, and H. W. den Hartog, Phys. Rev. B (to be published).

⁴A. D. Franklin and S. Marzullo, J. Phys. C **3**, L171 (1970).

⁵G. K. Miner, T. P. Graham, and G. T. Johnston, J. Chem. Phys. **57**, 1263 (1972).

⁶J. B. Fenn, J. C. Wright, and F. K. Fong, J. Chem.

Phys. **59**, 5591 (1973).

⁷W. B. Mims, *The Linear Electric Field Effect in Paramagnetic Resonance* (Clarendon, Oxford, 1976).

⁸A. Abragam and B. Bleaney, *Electron Paramagnetic Resonance of Transition Ions* (Clarendon Press, Oxford, 1970).

⁹C. A. Hutchison, B. R. Judd, and D. F. D. Pope, Proc. Phys. Soc. B **70**, 514 (1957).

¹⁰B. G. Wybourne, Phys. Rev. **148**, 317 (1966).

¹¹J. Owen and J. H. M. Thornley, Rep. Prog. Phys. **29**, 675 (1966).

- ¹²D. J. Newman, Adv. Phys. 20, 197 (1971).
¹³T. Oosterhoff and H. W. den Hartog, Phys. Status Solidi B 62, 469 (1974).
¹⁴H. Wever and H. W. den Hartog, Phys. Status Solidi B 70, 253 (1975).
¹⁵H. C. W. Beijerink and B. Willemsen, Physica (Utr.) 47, 515 (1970).
¹⁶Q. H. F. Vrehen and J. Volger, Physica (Utr.) 31, 845 (1965).
¹⁷D. J. Newman and W. Urban, Adv. Phys. 24, 793 (1975).
¹⁸A. Edgar and D. J. Newman, J. Phys. C 8, 4023 (1975).
¹⁹E. J. Bijvank and H. W. den Hartog, Phys. Rev. B 12, 4646 (1975).
²⁰J. Uhrin, Czech, J. Phys. B 23, 551 (1973).
²¹W. Low, Phys. Rev. 109, 265 (1958).
²²Ch. Ryter, Helv. Phys. Acta 30, 353 (1957).
²³M. V. Vlasova, N. G. Kakazei, and L. A. Sorin, Sov. Phys. Crystallogr. 19, 243 (1974).
²⁴S. B. Oseroff and R. Calvo, J. Phys. Chem. Solids 33, 2275 (1972).
²⁵M. Savostianova, Z. Phys. 64, 262 (1930).
²⁶W. T. Doyle, Phys. Rev. 111, 1067 (1958).
²⁷A. B. Scott, W. A. Smith, and M. A. Thomson, J. Phys. Chem. 57, 757 (1953).
²⁸M. Mayerl, S. B. Akad. Wiss. Wien Ila 160, 31 (1951).
²⁹H. W. den Hartog, thesis (Groningen, The Netherlands, 1969) (unpublished, copies are available).
³⁰C.-Y. Huang, Phys. Rev. 159, 683 (1967).
³¹A. Kiel, Phys. Rev. 148, 247 (1966).
³²J. I. Waber and D. T. Cromer, J. Chem. Phys. 42, 4116 (1965).
³³R. Parrot, Phys. Rev. B 9, 4660 (1974).
³⁴R. de Beer, R. Chatterjee, and R. P. J. Merks, J. Phys. C 9, 1539 (1976).
³⁵J. Andriessen (private communication).